PHYSICAL REVIEW D **96,** 036012 (2017)

$b \to (c,u)\tau\nu$ leptonic and semileptonic decays within an effective field theory approach

Rupak Dutta[1,*] and Anupama Bhol[2,†]

[1]*National Institute of Technology Silchar, Silchar 788010, India*
[2]*C. V. Raman College of Engineering, Bhubaneswar, Odisha 752054, India*

(Received 10 November 2016; published 25 August 2017)

The latest measurement of the ratio of branching ratios $R_D = \mathcal{B}(B \to D\tau\nu)/\mathcal{B}(B \to Dl\nu)$ and $R_{D^*} = \mathcal{B}(B \to D^*\tau\nu)/\mathcal{B}(B \to D^*l\nu)$, where l is either an electron or muon, differs from the standard model expectation by 1.9σ and 3.3σ, respectively. Similar tension has been observed in purely leptonic $B \to \tau\nu$ decays as well. In this context, we consider an effective field theory formalism in the presence of new physics to explore various new physics couplings. Motivated by the recently proposed new observables $R_D^\tau = R_D/\mathcal{B}(B \to \tau\nu)$ and $R_{D^*}^\tau = R_{D^*}/\mathcal{B}(B \to \tau\nu)$, we impose 2σ constraints from R_D^τ and $R_{D^*}^\tau$ in addition to the constraints from R_D, R_{D^*}, and $\mathcal{B}(B \to \tau\nu)$ to constrain the new physics parameter space. We study the impact of new physics on various observables related to $B_s \to (D_s, D_s^*)\tau\nu$ and $B \to \pi\tau\nu$ decay processes.

DOI: 10.1103/PhysRevD.96.036012

I. INTRODUCTION

Although the anomalies in the B meson decays suggest the presence of new physics (NP) in the flavor sector, NP had not yet been confirmed. Various model-dependent as well as model-independent analyses have been carried out to explore different NP scenarios. More specifically, the $b \to u$ and $b \to c$ leptonic and semileptonic decays of B mesons, such as $B \to (D, D^*)\tau\nu$, $B \to \pi\tau\nu$, and $B \to \tau\nu$ decays, have been the center of attention among the physics communities in the last few years [1–39]. Lately, various baryonic decay modes, such as $\Lambda_b \to \Lambda_c\tau\nu$ and $\Lambda_b \to p\tau\nu$ mediated via $b \to (c, u)\tau\nu$ transition processes, also received some attention because of the high production of Λ_b at the LHC [40–44]. The semileptonic B decays are sensitive probes to search for various NP models such as the two Higgs doublet model (2HDM), the minimal supersymmetric standard model (MSSM), and the leptoquark model. Exclusive semileptonic B decays were first observed by the Belle Collaboration [45], with subsequent studies reported by Belle [46,47] and *BABAR* [48,49]. The recent measurements on the ratio of branching ratios R_D and R_{D^*} are

$$\begin{aligned} R_D^{BABAR} &= 0.440 \pm 0.058 \pm 0.042, \\ R_{D^*}^{BABAR} &= 0.332 \pm 0.024 \pm 0.018, \\ R_D^{\text{Belle}} &= 0.375 \pm 0.064 \pm 0.026, \\ R_{D^*}^{\text{Belle}} &= 0.293 \pm 0.038 \pm 0.015, \end{aligned} \tag{1}$$

where the first uncertainty is statistical and the second one is systematic. Very recently, LHCb has also measured the ratio R_{D^*} to be $0.336 \pm 0.027 \pm 0.030$ [50]. Belle has reported its latest measurement on $R_{D^*} = 0.302 \pm 0.030 \pm 0.011$ with a semileptonic tagging method [51], which is within 1.6σ of the standard model (SM) theoretical expectation. The measured values of R_D and R_{D^*} exceed the SM prediction by 1.9σ and 3.3σ, respectively. Considering the R_D and R_{D^*} correlation, the combined analysis of R_D and R_{D^*} finds the deviation from the SM prediction to be at more than the 4.0σ level [52]. Combining results from the leptonic and hadronic decays of τ, the *BABAR* and Belle measured values of $\mathcal{B}(B \to \tau\nu)$ are $(1.83^{+0.53}_{-0.49}) \times 10^{-4}$ [53] and $(1.25 \pm 0.28) \times 10^{-4}$ [54], respectively. The Belle measurement is consistent with the SM prediction for both exclusive and inclusive V_{ub}, whereas, with the exclusive V_{ub}, there is still some discrepancy between the *BABAR* measured value of $\mathcal{B}(B \to \tau\nu)$ and the SM theoretical prediction.

Very recently, in Ref. [55], various new observables such as R_D^τ and $R_{D^*}^\tau$ have been proposed to explore the correlation between the new physics signals in $B \to (D, D^*)\tau\nu$ and $B \to \tau\nu$ decays. These observables,

$$R_D^\tau = \frac{R_D}{\mathcal{B}(B \to \tau\nu)}, \qquad R_{D^*}^\tau = \frac{R_{D^*}}{\mathcal{B}(B \to \tau\nu)}, \tag{2}$$

are obtained by dividing the ratio of branching ratios R_D and R_{D^*} by the $B \to \tau\nu$ branching ratio. Even though τ detection and identification systematics are present in $B \to \tau\nu$ and $B \to (D, D^*)\tau\nu$ decays, it will mostly cancel in these newly constructed ratios. However, these ratios suffer from large uncertainties due to the presence of the not very well-known parameter V_{ub} in the denominator. The estimated values are [55]

*rupak@phy.nits.ac.in
†anupama.phy@gmail.com

$$R_D^{\tau\,BABAR}(\times 10^3) = 2.404 \pm 0.838,$$
$$R_{D^*}^{\tau\,BABAR}(\times 10^3) = 1.814 \pm 0.582,$$
$$R_D^{\tau\,\mathrm{Belle}}(\times 10^3) = 3.0 \pm 1.1,$$
$$R_{D^*}^{\tau\,\mathrm{Belle}}(\times 10^3) = 2.344 \pm 0.799. \quad (3)$$

The estimated values of these new observables from *BABAR* and Belle measured values of the ratio of branching ratios R_D, R_{D^*}, and $\mathcal{B}(B \to \tau\nu)$ are consistent with the SM prediction [55], although the measured values of R_D and R_{D^*} differ from the SM prediction. However, it does not necessarily rule out the possibility of the presence of NP because, even if NP is present, its effect may largely cancel in the ratios. In Ref. [55], the authors discuss the constraints on 2HDM parameter space using the constraints from the estimated values of R_D^τ and $R_{D^*}^\tau$ and find that, although the *BABAR* data do not allow a simultaneous explanation of all the above-mentioned deviations, for Belle data, there is actually a common allowed parameter space. In the present study, we use an effective field theory formalism in the presence of NP to explore various NP effects on $b \to u$ and $b \to c$ leptonic and semileptonic decays. This is indeed a model-dependent approach since the NP Wilson coefficients pertaining to $b \to u$ and $b \to c$ transitions are related by the ratio of corresponding CKM matrix elements only. Our main motivation is to find whether it is possible to unravel useful information regarding the various Lorentz structures of beyond-the-SM physics from the estimated values of R_D^τ and $R_{D^*}^\tau$ since these values are consistent with the SM prediction. To realize this, we first consider the constraints from the measured values of R_D, R_{D^*}, and $\mathcal{B}(B \to \tau\nu)$ to constrain the NP parameter space. Second, we impose additional constraints from the estimated values of R_D^τ and $R_{D^*}^\tau$ to further constrain or exclude the NP parameter space that is preferred by the measured values of R_D, R_{D^*}, and $\mathcal{B}(B \to \tau\nu)$. We make a comparative analysis of *BABAR* and Belle data and give a prediction on various observables related to $B \to \pi\tau\nu$ and $B_s \to (D_s, D_s^*)\tau\nu$ decays.

Our paper is organized as follows. In Sec. II, we start with a brief description of the effective Lagrangian for the $b \to (u, c)l\nu$ transition decays in the presence of NP. All the relevant formulas, such as the partial decay width of $B \to l\nu$ decays and differential decay width of three-body $B \to (P, V)l\nu$ decays, are reported in Sec. II. We also construct various new observables related to semileptonic B and B_s meson decays. In Sec. III, we start with the input parameters that are used for our numerical computation. The SM prediction and the effect of each NP coupling on various observables related to semileptonic B and B_s meson decays are reported in Sec. III. We conclude with a brief summary of our results in Sec. IV.

II. HELICITY AMPLITUDES WITHIN THE EFFECTIVE FIELD THEORY APPROACH

In the presence of NP, the effective weak Lagrangian for the $b \to q' l\nu$ transition decays, where q' is either a u quark or a c quark, can be written as [56,57]

$$\mathcal{L}_{\mathrm{eff}} = -\frac{4G_F}{\sqrt{2}} V_{q'b}\{(1+V_L)\bar{l}_L\gamma_\mu\nu_L\bar{q'}_L\gamma^\mu b_L + V_R\bar{l}_L\gamma_\mu\nu_L\bar{q'}_R\gamma^\mu b_R + \tilde{V}_L\bar{l}_R\gamma_\mu\nu_R\bar{q'}_L\gamma^\mu b_L + \tilde{V}_R\bar{l}_R\gamma_\mu\nu_R\bar{q'}_R\gamma^\mu b_R + S_L\bar{l}_R\nu_L\bar{q'}_R b_L$$
$$+ S_R\bar{l}_R\nu_L\bar{q'}_L b_R + \tilde{S}_L\bar{l}_L\nu_R\bar{q'}_R b_L + \tilde{S}_R\bar{l}_L\nu_R\bar{q'}_L b_R + T_L\bar{l}_R\sigma_{\mu\nu}\nu_L\bar{q'}_R\sigma^{\mu\nu} b_L + \tilde{T}_L\bar{l}_L\sigma_{\mu\nu}\nu_R\bar{q'}_L\sigma^{\mu\nu} b_R\} + \mathrm{H.c.}, \quad (4)$$

where G_F is the Fermi coupling constant and $V_{q'b}$ is the CKM matrix element. The vector-, scalar-, and tensor-type NP interactions denoted by $V_{L,R}$, $S_{L,R}$, and T_L are associated with left-handed neutrinos, whereas $\tilde{V}_{L,R}$-, $\tilde{S}_{L,R}$-, and $\tilde{T}_L$-type NP couplings are associated with right-handed neutrinos. We consider all the NP couplings to be real for our analysis. Again, we keep only vector- and scalar-type NP couplings in our analysis. We rewrite the effective Lagrangian as [25]

$$\mathcal{L}_{\mathrm{eff}} = -\frac{G_F}{\sqrt{2}} V_{q'b}\{G_V\bar{l}\gamma_\mu(1-\gamma_5)\nu_l\bar{q'}\gamma^\mu b - G_A\bar{l}\gamma_\mu(1-\gamma_5)\nu_l\bar{q'}\gamma^\mu\gamma_5 b + G_S\bar{l}(1-\gamma_5)\nu_l\bar{q'}b$$
$$- G_P\bar{l}(1-\gamma_5)\nu_l\bar{q'}\gamma_5 b + \tilde{G}_V\bar{l}\gamma_\mu(1+\gamma_5)\nu_l\bar{q'}\gamma^\mu b - \tilde{G}_A\bar{l}\gamma_\mu(1+\gamma_5)\nu_l\bar{q'}\gamma^\mu\gamma_5 b$$
$$+ \tilde{G}_S\bar{l}(1+\gamma_5)\nu_l\bar{q'}b - \tilde{G}_P\bar{l}(1+\gamma_5)\nu_l\bar{q'}\gamma_5 b\} + \mathrm{H.c.}, \quad (5)$$

where

$$G_V = 1 + V_L + V_R, \qquad G_A = 1 + V_L - V_R, \qquad G_S = S_L + S_R, \qquad G_P = S_L - S_R$$
$$\tilde{G}_V = \tilde{V}_L + \tilde{V}_R, \qquad \tilde{G}_A = \tilde{V}_L - \tilde{V}_R, \qquad \tilde{G}_S = \tilde{S}_L + \tilde{S}_R, \qquad \tilde{G}_P = \tilde{S}_L - \tilde{S}_R.$$

The SM contribution can be obtained once we set $V_{L,R} = S_{L,R} = \tilde{V}_{L,R} = \tilde{S}_{L,R} = 0$ in Eq. (5). In the presence of NP, the partial decay width of $B \to l\nu$ and differential decay width of three-body $B_q \to (P,V)l\nu$ decays, where P is a pseudoscalar meson and V is a vector meson, can be expressed as [25]

$$\Gamma(B \to l\nu) = \frac{G_F^2|V_{ub}|^2}{8\pi} f_B^2 m_l^2 m_B \left(1 - \frac{m_l^2}{m_B^2}\right)^2 \left\{ \left[G_A - \frac{m_B^2}{m_l(m_b(\mu) + m_u(\mu))} G_P \right]^2 + \left[\tilde{G}_A - \frac{m_B^2}{m_l(m_b(\mu) + m_u(\mu))} \tilde{G}_P \right]^2 \right\}, \tag{6}$$

$$\frac{d\Gamma^P}{dq^2} = \frac{8N|\vec{p}_P|}{3} \left\{ H_0^2 (G_V^2 + \tilde{G}_V^2) \left(1 + \frac{m_l^2}{2q^2}\right) + \frac{3m_l^2}{2q^2} \left[\left(H_t G_V + \frac{\sqrt{q^2}}{m_l} H_S G_S \right)^2 + \left(H_t \tilde{G}_V + \frac{\sqrt{q^2}}{m_l} H_S \tilde{G}_S \right)^2 \right] \right\} \tag{7}$$

and

$$\frac{d\Gamma^V}{dq^2} = \frac{8N|\vec{p}_V|}{3} \left\{ \mathcal{A}_{AV}^2 + \frac{m_l^2}{2q^2}[\mathcal{A}_{AV}^2 + 3\mathcal{A}_{tP}^2] + \tilde{\mathcal{A}}_{AV}^2 + \frac{m_l^2}{2q^2}[\tilde{\mathcal{A}}_{AV}^2 + 3\tilde{\mathcal{A}}_{tP}^2] \right\} \tag{8}$$

where

$$\begin{aligned}
|\vec{p}_{(P,V)}| &= \sqrt{\lambda(m_{B_q}^2, m_{(P,V)}^2, q^2)}/2m_{B_q}, \qquad \lambda(a,b,c) = a^2 + b^2 + c^2 - 2(ab + bc + ca) \\
N &= \frac{G_F^2|V_{q'b}|^2 q^2}{256\pi^3 m_{B_q}^2} \left(1 - \frac{m_l^2}{q^2}\right)^2, \qquad H_0 = \frac{2m_{B_q}|\vec{p}_P|}{\sqrt{q^2}} F_+(q^2) \\
H_t &= \frac{m_{B_q}^2 - m_P^2}{\sqrt{q^2}} F_0(q^2), \qquad H_S = \frac{m_{B_q}^2 - m_P^2}{m_b(\mu) - m_{q'}(\mu)} F_0(q^2), \\
\mathcal{A}_{AV}^2 &= \mathcal{A}_0^2 G_A^2 + \mathcal{A}_\parallel^2 G_A^2 + \mathcal{A}_\perp^2 G_V^2, \qquad \tilde{\mathcal{A}}_{AV}^2 = \mathcal{A}_0^2 \tilde{G}_A^2 + \mathcal{A}_\parallel^2 \tilde{G}_A^2 + \mathcal{A}_\perp^2 \tilde{G}_V^2 \\
\mathcal{A}_{tP} &= \mathcal{A}_t G_A + \frac{\sqrt{q^2}}{m_l} \mathcal{A}_P G_P, \qquad \tilde{A}_{tP} = \mathcal{A}_t \tilde{G}_A + \frac{\sqrt{q^2}}{m_l} \mathcal{A}_P \tilde{G}_P,
\end{aligned} \tag{9}$$

and

$$\begin{aligned}
\mathcal{A}_0 &= \frac{1}{2m_V\sqrt{q^2}} \left[(m_{B_q}^2 - m_V^2 - q^2)(m_{B_q} + m_V) A_1(q^2) - \frac{4m_{B_q}^2 |\vec{p}_V|^2}{m_{B_q} + m_V} A_2(q^2) \right], \\
\mathcal{A}_\parallel &= \frac{2(m_{B_q} + m_V) A_1(q^2)}{\sqrt{2}}, \qquad \mathcal{A}_\perp = -\frac{4m_{B_q} V(q^2) |\vec{p}_V|}{\sqrt{2}(m_{B_q} + m_V)}, \\
\mathcal{A}_t &= \frac{2m_{B_q}|\vec{p}_V| A_0(q^2)}{\sqrt{q^2}}, \qquad \mathcal{A}_P = -\frac{2m_{B_q}|\vec{p}_V| A_0(q^2)}{(m_b(\mu) + m_c(\mu))}.
\end{aligned} \tag{10}$$

For the details of the helicity amplitudes, the B meson decay constant, and the $B_q \to (P,V)$ meson transition form factors, we refer to Refs. [25,58].

Semileptonic B_s decays to $D_s\tau\nu$ and $D_s^*\tau\nu$ and B decays to $\pi\tau\nu$ are also mediated via $b \to (u,c)\tau\nu$ quark-level transition processes and, in principle, are subject to NP. In this context, we define the ratio of branching ratios in these decay modes similar to $B \to (D, D^*)\tau\nu$ decays, which are

$$\begin{aligned}
R_\pi &= \frac{\mathcal{B}(B \to \pi\tau\nu)}{\mathcal{B}(B \to \pi l\nu)}, \qquad R_{D_s} = \frac{\mathcal{B}(\bar{B}_s \to D_s\tau^-\bar{\nu}_\tau)}{\mathcal{B}(\bar{B}_s \to D_s l^-\bar{\nu}_l)}, \\
R_{D_s^*} &= \frac{\mathcal{B}(\bar{B}_s \to D_s^*\tau^-\bar{\nu}_\tau)}{\mathcal{B}(\bar{B}_s \to D_s^* l^-\bar{\nu}_l)}, \qquad R_\pi^\tau = \frac{\mathcal{B}(B \to \pi\tau\nu)}{\mathcal{B}(B \to \tau\nu)}, \\
R_{D_s}^\tau &= \frac{R_{D_s}}{\mathcal{B}(B \to \tau\nu)}, \qquad R_{D_s^*}^\tau = \frac{R_{D_s^*}}{\mathcal{B}(B \to \tau\nu)}.
\end{aligned} \tag{11}$$

We want to mention that although R_π, R_{D_s}, $R_{D_s^*}$, and R_π^τ do not depend on CKM matrix elements V_{ub} and V_{cb}, the newly constructed ratios $R_{D_s}^\tau$ and $R_{D_s^*}^\tau$ do depend on the CKM matrix element V_{ub}. We note that our definition of R_π^τ is different from that of $R_\pi/\mathcal{B}(B \to \tau\nu)$. The V_{ub} dependency cancels in the former; however, it remains in the latter definition.

We wish to see the effect of NP couplings on various observables related to $b \to u$ and $b \to c$ leptonic and

semileptonic decays. There are two types of uncertainties in the theoretical calculation of the observables. The first kind of uncertainties may come from the very well-known input parameters, such as quark masses, meson masses, and the mean lifetime of mesons. We ignore such uncertainties as they are not important for our analysis. The second kind of uncertainties may arise because of the not very well-known parameters, such as CKM matrix elements, meson decay constants, and the meson-to-meson transition form factors. In order to gauge the effect of the above-mentioned uncertainties on various observables, we use a random number generator and perform a random scan of all the theoretical inputs such as CKM matrix elements, meson decay constants, and the meson-to-meson transition form

TABLE I. Theory input parameters.

CKM matrix elements		Meson decay constants (in GeV)	
$\lvert V_{ub}\rvert$ (exclusive)	$(3.61 \pm 0.32) \times 10^{-3}$ [60]	f_B	0.1906 ± 0.0047 [61–63]
$\lvert V_{cb}\rvert$ (average)	$(40.9 \pm 1.1) \times 10^{-3}$ [60]		
Inputs for $(B \to \pi)$ form factors		Inputs for $(B \to D^*)$ form factors	
$F_+(0) = F_0(0)$	0.281 ± 0.028 [64]	$h_{A_1}(1)\lvert V_{cb}\rvert$	$(34.6 \pm 1.02) \times 10^{-3}$ [65]
b_1	-1.62 ± 0.70 [64]	ρ_1^2	1.214 ± 0.035 [65]
b_1^0	-3.98 ± 0.97 [64]	$R_1(1)$	1.401 ± 0.038 [65]
Inputs for $(B \to D)$ form factors		$R_2(1)$	0.864 ± 0.025 [65]
$V_1(1)\lvert V_{cb}\rvert$	$(43.0 \pm 2.36) \times 10^{-3}$ [66]	$R_0(1)$	1.14 ± 0.114 [2]
ρ_1^2	1.20 ± 0.098 [66]		

Inputs for $(B_s \to D_s)$ form factors [67]

	F_+	F_0
$F(0)$	0.74 ± 0.02	0.74 ± 0.02
σ_1	0.20 ± 0.02	0.430 ± 0.043
σ_2	-0.461 ± 0.0461	-0.464 ± 0.0464

Inputs for $(B_s \to D_s^*)$ form factors [67]

	V	A_0	A_1	A_2
$F(0)$	0.95 ± 0.02	0.67 ± 0.01	0.70 ± 0.01	0.75 ± 0.02
σ_1	0.372 ± 0.0372	0.350 ± 0.035	0.463 ± 0.0463	1.04 ± 0.104
σ_2	$-0.561 \pm .0561$	-0.60 ± 0.06	-0.510 ± 0.051	-0.07 ± 0.007

TABLE II. Experimental input parameters.

Experiment	Observable	Central value $\pm 1\sigma$	2σ range
BABAR	$\mathcal{B}(B \to \tau\nu)$	$(1.83 \pm 0.52) \times 10^{-4}$ [53]	$(0.79, 2.82) \times 10^{-4}$
Belle	$\mathcal{B}(B \to \tau\nu)$	$(1.25 \pm 0.28) \times 10^{-4}$ [54]	$(0.69, 1.81) \times 10^{-4}$
BABAR	R_D	0.440 ± 0.072 [48,49]	(0.296,0.584)
BABAR	R_{D^*}	0.332 ± 0.030 [48,49]	(0.272,0.392)
Belle	R_D	0.375 ± 0.069 [47]	(0.237,0.513)
Belle	R_{D^*}	$0.293 \pm 0.0.041$ [47]	(0.211,0.375)
BABAR	R_D^τ	$(2.404 \pm 0.838) \times 10^3$ [55]	$(0.728, 4.080) \times 10^3$
BABAR	$R_{D^*}^\tau$	$(1.814 \pm 0.582) \times 10^3$ [55]	$(0.650, 2.978) \times 10^3$
Belle	R_D^τ	$(3.0 \pm 1.1) \times 10^3$ [55]	$(0.800, 5.200) \times 10^3$
Belle	$R_{D^*}^\tau$	$(2.344 \pm 0.799) \times 10^3$ [55]	$(0.746, 3.942) \times 10^3$

TABLE III. SM prediction of various observables.

Observable	Central value	1σ range	Observable	Central value	1σ range
R_D^τ	3.737×10^3	$(2.889, 4.919) \times 10^3$	$R_{D_s}^\tau$	3.270×10^3	$(2.499, 4.396) \times 10^3$
$R_{D^*}^\tau$	3.022×10^3	$(2.375, 3.918) \times 10^3$	$R_{D_s^*}^\tau$	2.881×10^3	$(2.295, 3.687) \times 10^3$
R_π^τ	1.33	(0.847,2.015)	R_{D_s}	0.274	(0.255,0.295)
R_π	0.698	(0.654,0.764)	$R_{D_s^*}$	0.241	(0.236,0.246)

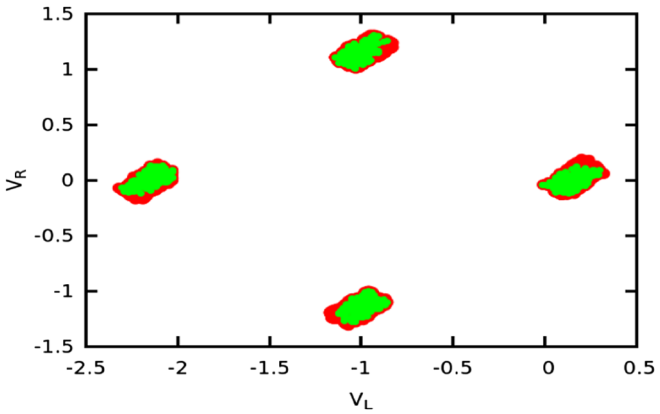

FIG. 1. Allowed ranges in V_L and V_R NP couplings after the *BABAR* 2σ experimental constraint is imposed. The dark (red) region corresponds to the allowed ranges after the R_D, R_{D^*}, and $\mathcal{B}(B \to \tau\nu)$ constraints are imposed, whereas the light (green) region corresponds to the allowed ranges of V_L and V_R after additional 2σ constraints from R_D^τ and $R_{D^*}^\tau$ are imposed.

factors. We vary all the theoretical inputs within 1σ from their central values in our random scan. The allowed NP parameter space is obtained by imposing 2σ constraints from *BABAR* and Belle measured values of the ratio of branching ratios R_D, R_{D^*}, and $\mathcal{B}(B \to \tau\nu)$. We also use 2σ constraints from the estimated values of R_D^τ and $R_{D^*}^\tau$ to restrict the NP parameter space even further. We now proceed to discuss the results of our analysis.

III. NUMERICAL CALCULATIONS

For definiteness, let us first give the details of the input parameters that are used for the theoretical computation of all the observables. For the quark mass, meson mass, and the meson lifetime, we use the following input parameters from Ref. [59]:

$$\begin{aligned} m_b(m_b) &= 4.18\ \text{GeV}, & m_c(m_b) &= 0.91\ \text{GeV}, \\ m_\pi &= 0.13957\ \text{GeV} & m_{B^-} &= 5.27925\ \text{GeV}, \\ m_{B^0} &= 5.27955\ \text{GeV}, & m_{B_s} &= 5.36677\ \text{GeV}, \\ m_{D^0} &= 1.86486\ \text{GeV}, & m_{D^{*0}} &= 2.00698\ \text{GeV}, \\ m_{D_s^+} &= 1.9685\ \text{GeV}, & m_{D_s^{*+}} &= 2.1123\ \text{GeV}, \\ \tau_{B^0} &= 1.519 \times 10^{-12}\ \text{s} & \tau_{B^-} &= 1.641 \times 10^{-12}\ \text{s}, \\ \tau_{B_s} &= 1.516 \times 10^{-12}\ \text{s} \end{aligned} \tag{12}$$

Similarly, for the CKM matrix elements, meson decay constant, and meson-to-meson transition form factors, we use the inputs in Table I. We refer to Refs. [25,58] for a detailed discussion on various form factor calculations. The uncertainties associated with both the theory and experimental input parameters are added in quadrature and shown in Tables I and II. The SM predictions for all the

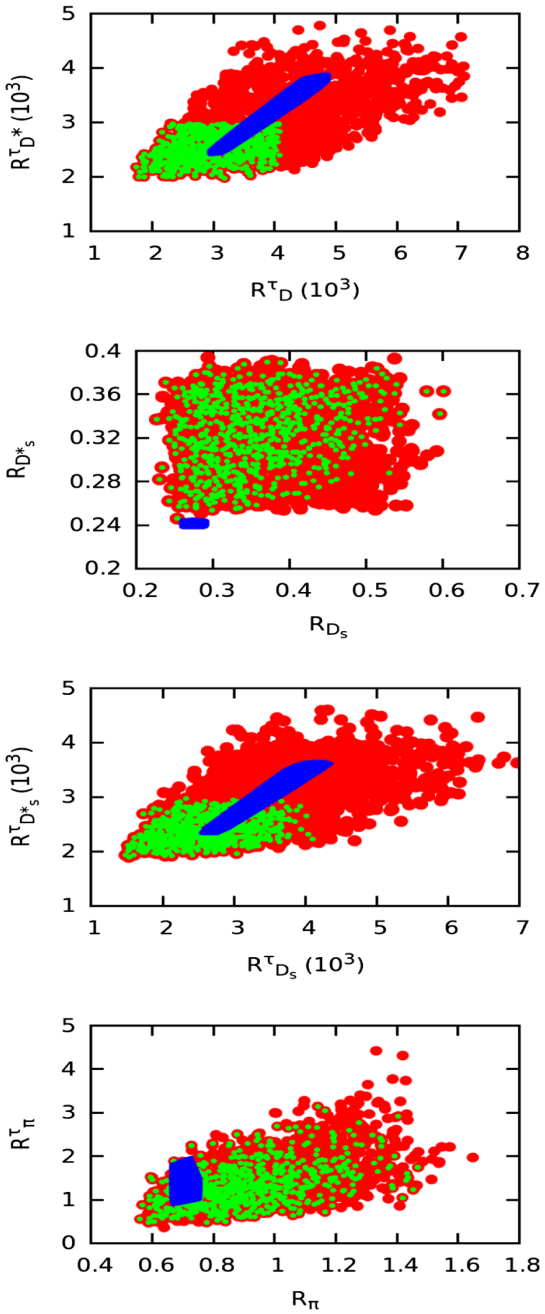

FIG. 2. Allowed ranges in various observables with the V_L and V_R NP couplings of Fig. 1. The dark (red) region corresponds to the allowed ranges after R_D, R_{D^*}, and $\mathcal{B}(B \to \tau\nu)$ constraints are imposed, whereas the light (green) region corresponds to the allowed ranges of the observables after additional 2σ constraints from R_D^τ and $R_{D^*}^\tau$ are imposed. The blue region corresponds to the 1σ allowed range within the SM.

observables are reported in Table III. Central values of all the observables are obtained by using the central values of all the input parameters from Eq. (12) and from Table I. The 1σ range in each observable, reported in Table III, is obtained by performing a random scan of all the theory inputs such as B_q meson decay constants, $B_q \to (P,V)$

TABLE IV. Allowed ranges in various observables with (V_L, V_R) NP couplings of Fig. 1. The ranges reported in Column I represent the allowed values of each observable after constraints from *BABAR* measured values of R_D, R_{D^*}, and $\mathcal{B}(B \to \tau\nu)$ are imposed, whereas the ranges in Column II represent the allowed values after additional 2σ constraints from R^τ_D and $R^\tau_{D^*}$ are imposed.

Observable	Column I	Column II	Observable	Column I	Column II
$R^\tau_D(\times 10^3)$	(1.736, 7.097)	(1.736, 4.080)	R^τ_π	(0.359, 4.422)	(0.472, 3.144)
$R^\tau_{D^*}(\times 10^3)$	(1.978, 4.780)	(1.978, 2.978)	R_π	(0.560, 1.648)	(0.560, 1.469)
$R^\tau_{D_s}(\times 10^3)$	(1.480, 6.973)	(1.480, 4.101)	R_{D_s}	(0.226, 0.601)	(0.226, 0.601)
$R^\tau_{D^*_s}(\times 10^3)$	(1.895, 4.599)	(1.895, 2.980)	$R_{D^*_s}$	(0.246, 0.394)	(0.246, 0.390)

transition form factors, and the CKM matrix elements $|V_{qb}|$ within 1σ of their central values.

Our main aim is to study NP effects on various new observables such as R_π, R_{D_s}, $R_{D^*_s}$, R^τ_D, $R^\tau_{D^*}$, R^τ_π, $R^\tau_{D_s}$, and $R^\tau_{D^*_s}$. We consider four different NP scenarios. First, we use 2σ experimental constraints from the *BABAR* and Belle measured values of the ratio of branching ratios R_D and R_{D^*}, and $\mathcal{B}(B \to \tau\nu)$. Second, we add an additional constraint coming from R^τ_D and $R^\tau_{D^*}$ since the estimated values of these new ratios are consistent with the SM prediction. Although, at present, the estimated errors on both these observables are rather large, this could be reduced after more precise data on V_{ub} are available. In view of the anticipated improved precision in the measurement of V_{ub}, we impose 2σ experimental constraints from the estimated values of R^τ_D and $R^\tau_{D^*}$, in addition to the constraints from R_D, R_{D^*}, and $\mathcal{B}(B \to \tau\nu)$, to explore various NP couplings. All the NP parameters are considered to be real for our analysis. We also assume that only the third-generation leptons get contributions from the NP couplings in the $b \to (u, c)l\nu$ processes, and for $l = e^-, \mu^-$ cases, NP is absent. We next discuss the effect of various NP couplings

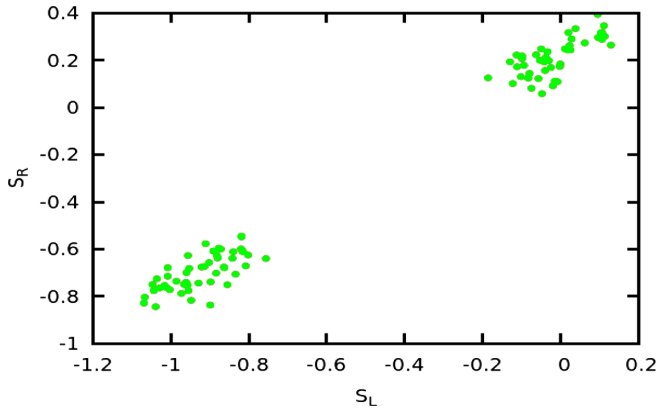

FIG. 3. Allowed ranges in S_L and S_R NP couplings after the *BABAR* 2σ experimental constraint is imposed. We note that the allowed range denoted by dark (red) dots obtained by imposing the 2σ constraint from R_D, R_{D^*}, and $\mathcal{B}(B \to \tau\nu)$ overlaps with the allowed range denoted by light (green) dots after additional 2σ constraints from R^τ_D and $R^\tau_{D^*}$ are imposed. In this scenario, R^τ_D and $R^\tau_{D^*}$ do not constrain the NP parameter space any further.

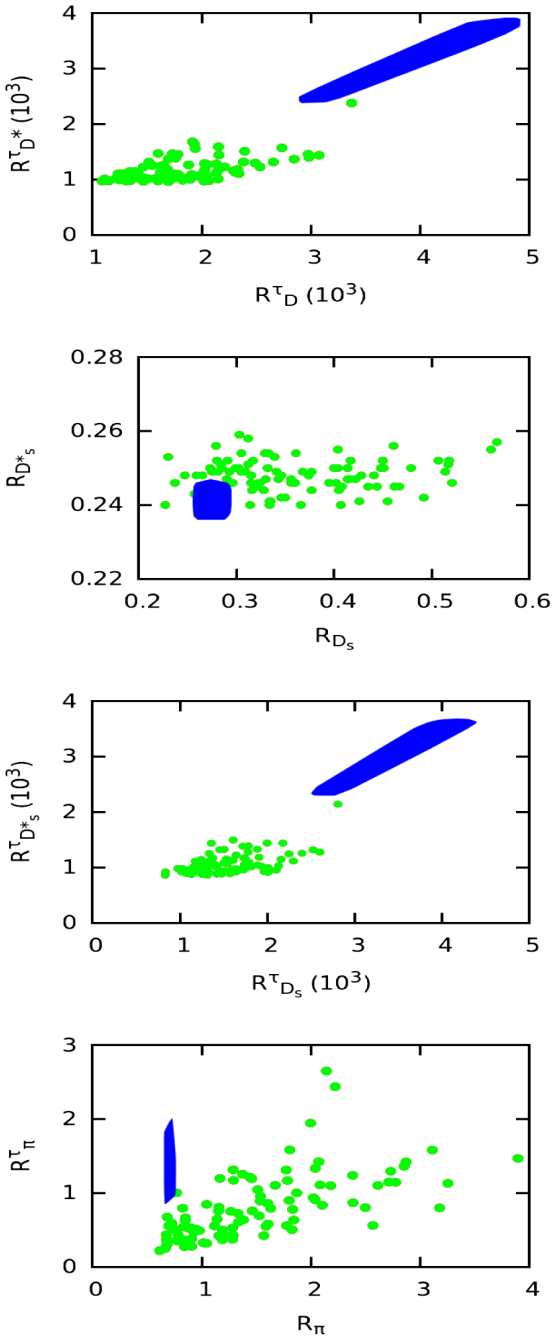

FIG. 4. Allowed ranges in various observables are shown by light (green) dots with the S_L and S_R NP couplings of Fig. 3. The blue region corresponds to the 1σ allowed range within the SM.

TABLE V. Allowed ranges in various observables with (S_L, S_R) NP couplings of Fig. 3. The ranges reported in Column I represent the allowed values of each observable after constraints from *BABAR* measured values of R_D, R_{D^*}, and $\mathcal{B}(B \to \tau\nu)$ are imposed. Column II represents the allowed range in each observable after additional 2σ constraints from R^τ_D and $R^\tau_{D^*}$ are imposed.

Observable	Column I	Column II	Observable	Column I	Column II
$R^\tau_D(\times 10^3)$	(1.087, 3.374)	(1.087, 3.374)	R^τ_π	(0.221, 2.650)	(0.221, 2.650)
$R^\tau_{D^*}(\times 10^3)$	(0.962, 2.378)	(0.962, 2.378)	R_π	(0.615, 3.898)	(0.615, 3.898)
$R^\tau_{D_s}(\times 10^3)$	(0.831, 2.810)	(0.831, 2.810)	R_{D_s}	(0.227, 0.567)	(0.227, 0.567)
$R^\tau_{D^*_s}(\times 10^3)$	(0.863, 2.142)	(0.863, 2.142)	$R_{D^*_s}$	(0.240, 0.259)	(0.240, 0.259)

after imposing constraints from *BABAR* and Belle measurements.

A. *BABAR* constraint

We consider four different NP scenarios for our analysis. In the first scenario, we vary new vector couplings V_L and V_R and consider all other NP couplings to be zero. First, we impose 2σ experimental constraints from *BABAR* measured values of the ratio of branching ratios R_D, R_{D^*}, and $\mathcal{B}(B \to \tau\nu)$ to constrain the new vector-type coupling (V_L, V_R). Second, we impose additional 2σ constraints from the estimated values of R^τ_D and $R^\tau_{D^*}$ to see whether it is possible to constrain the NP parameter space even further. The allowed ranges of new vector couplings V_L and V_R are shown in Fig. 1. The dark (red) regions correspond to the allowed ranges of V_L and V_R that are obtained once the 2σ constraint from the measured values of R_D, R_{D^*}, and $\mathcal{B}(B \to \tau\nu)$ is imposed. Similarly, the light (green) region corresponds to the allowed ranges of the new vector couplings V_L and V_R after an additional 2σ constraint from the estimated values of R^τ_D and $R^\tau_{D^*}$ is imposed. It is clear that the additional constraint from R^τ_D and $R^\tau_{D^*}$ does exclude some outer regions of the NP parameter space that

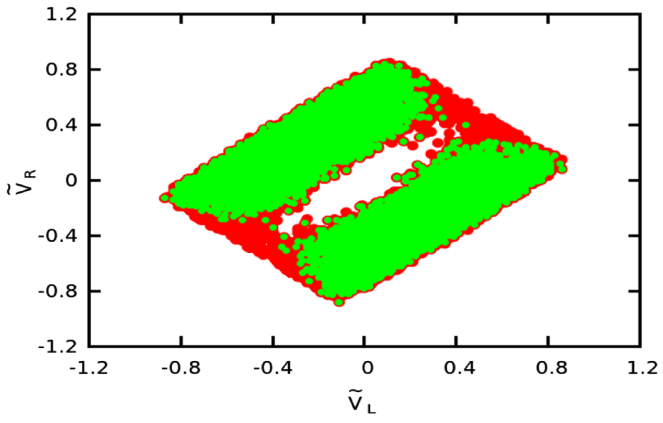

FIG. 5. Allowed ranges in $\tilde{V}_L$ and $\tilde{V}_R$ NP couplings after the *BABAR* 2σ experimental constraint is imposed. The dark (red) region corresponds to the allowed ranges after the R_D, R_{D^*}, and $\mathcal{B}(B \to \tau\nu)$ constraints are imposed, whereas the light (green) region corresponds to the allowed ranges of $\tilde{V}_L$ and $\tilde{V}_R$ after additional 2σ constraints from R^τ_D and $R^\tau_{D^*}$ are imposed.

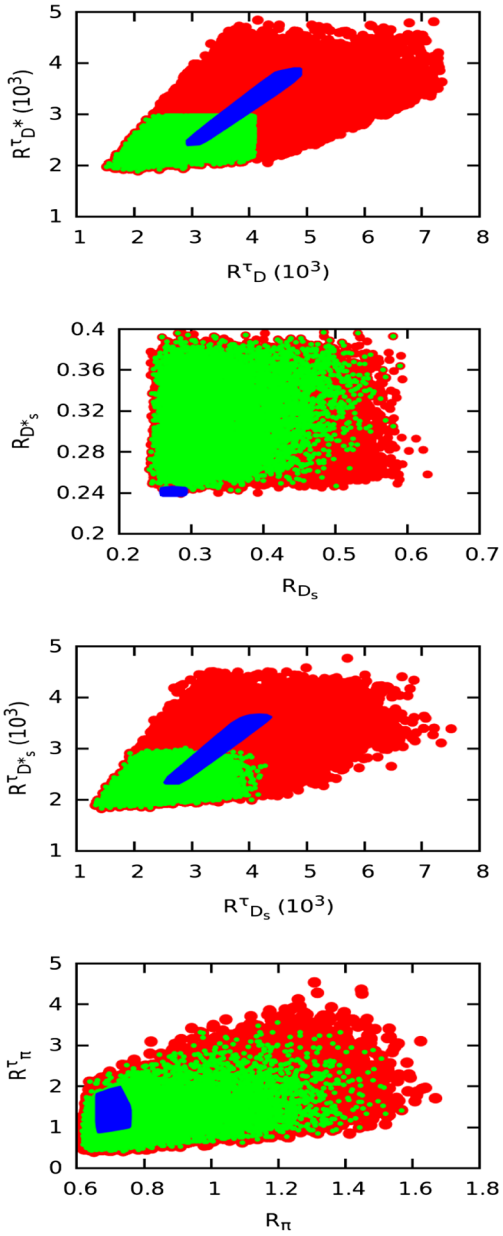

FIG. 6. Allowed ranges in various observables with $\tilde{V}_L$ and $\tilde{V}_R$ NP couplings of Fig. 5. We show in dark (red) the allowed ranges after 2σ constraints from R_D, R_{D^*}, and $\mathcal{B}(B \to \tau\nu)$ are imposed. Similarly, the allowed ranges are shown in light (green) after additional 2σ constraints from R^τ_D and $R^\tau_{D^*}$ are imposed. The blue region corresponds to the 1σ allowed range within the SM.

TABLE VI. Allowed ranges in various observables with $(\tilde{V}_L, \tilde{V}_R)$ NP couplings of Fig. 5. The ranges reported in Column I represent the allowed values of each observable after constraints from *BABAR* measured values of R_D, R_{D^*}, and $\mathcal{B}(B \to \tau\nu)$ are imposed. Column II represents the allowed range in each observable after additional 2σ constraints from R_D^τ and $R_{D^*}^\tau$ are imposed.

Observable	Column I	Column II	Observable	Column I	Column II
$R_D^\tau(\times 10^3)$	(1.521, 7.346)	(1.521, 4.080)	R_π^τ	(0.398, 4.538)	(0.414, 3.563)
$R_{D^*}^\tau(\times 10^3)$	(1.889, 4.841)	(1.889, 2.978)	R_π	(0.617, 1.669)	(0.617, 1.568)
$R_{D_s}^\tau(\times 10^3)$	(1.323, 7.508)	(1.323, 4.275)	R_{D_s}	(0.241, 0.628)	(0.241, 0.590)
$R_{D_s^*}^\tau(\times 10^3)$	(1.826, 4.767)	(1.826, 3.008)	$R_{D_s^*}$	(0.239, 0.397)	(0.241, 0.397)

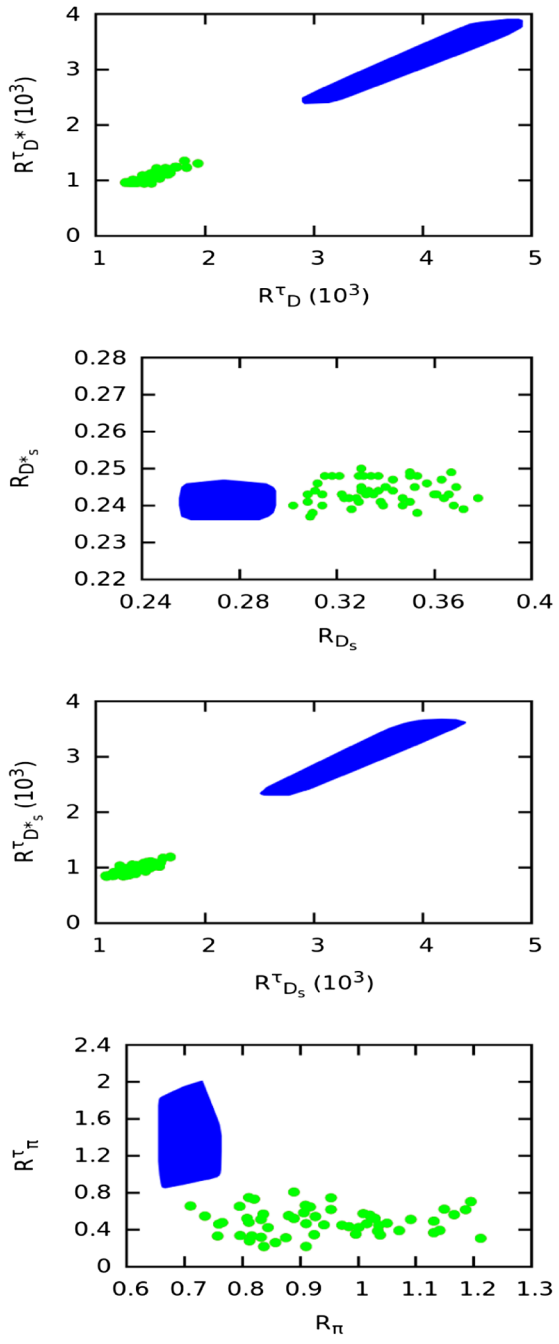

FIG. 7. Allowed ranges in various observables are shown in light (green) dots with $\tilde{S}_L$ and $\tilde{S}_R$ NP couplings. The blue region corresponds to the 1σ allowed range within the SM.

is preferred by R_D, R_{D^*}, and $\mathcal{B}(B \to \tau\nu)$. More precise data on V_{ub} in the future will definitely help constrain the NP parameter space even further.

In Fig. 2, we show the NP effect on various observables after imposing the 2σ experimental constraint from the *BABAR* measured values. We show with dark (red) dots the NP effect on various observables after 2σ constraints from the measured values of R_D, R_{D^*}, and $\mathcal{B}(B \to \tau\nu)$ are imposed. Again, we show with light (green) dots the NP effect after additional 2σ constraints from R_D^τ and $R_{D^*}^\tau$ are imposed. The allowed ranges in each observable are shown in Table IV. Although we find significant deviation of all the observables from SM expectations in this scenario, the deviation from the SM prediction is seen to be more pronounced in the case of R_{D_s} and $R_{D_s^*}$. It is observed that the allowed ranges in $R_{D_s}^\tau$, $R_{D_s^*}^\tau$, and R_π^τ are reduced, whereas there are no or very little changes in R_π, R_{D_s}, and $R_{D_s^*}$ allowed ranges after the additional 2σ constraints from R_D^τ and $R_{D^*}^\tau$ are imposed. We want to emphasize that the NP effect will not be present in $R_{D_{(s)}^{(*)}}^\tau$ and R_π^τ if only V_L-type NP couplings are present. In that case, $G_V = G_A$, and the contribution from the NP couplings will cancel in these ratios.

In the second scenario, we study the impact of new scalar couplings S_L and S_R on various observables. To do this, we vary S_L and S_R and perform a random scan over all theoretical input parameters within 1σ of their central values. We impose 2σ constraints from the *BABAR* measured values to determine the allowed ranges of the new scalar couplings S_L and S_R, which is shown in Fig. 3. It should be noted that the allowed range obtained by imposing 2σ constraints from R_D, R_{D^*}, and $\mathcal{B}(B \to \tau\nu)$ overlaps with the allowed range after additional 2σ constraints from R_D^τ and $R_{D^*}^\tau$ are imposed. Additional constraints from the estimated values of R_D^τ and $R_{D^*}^\tau$ do not constrain the NP parameter space any further. Hence, unlike Fig. 1, we observe only one set of data points, which are shown with light (green) dots. The effect of S_L- and S_R-type NP couplings on various observables are shown in Fig. 4 after the 2σ experimental constraints from *BABAR* measured values are imposed. Significant deviation from the SM expectation is observed in this scenario. Again, additional 2σ constraints from R_D^τ and $R_{D^*}^\tau$ do not

TABLE VII. Allowed ranges in various observables with $(\tilde{S}_L, \tilde{S}_R)$ NP couplings. The values reported in Column I represent the allowed values of each observable after constraints from *BABAR* measured values of R_D, R_{D^*}, and $\mathcal{B}(B \to \tau\nu)$ are imposed. Column II represents the allowed range in each observable after additional 2σ constraints from R_D^τ and $R_{D^*}^\tau$ are imposed.

Observable	Column I	Column II	Observable	Column I	Column II
$R_D^\tau(\times 10^3)$	(1.270, 1.936)	(1.270, 1.936)	R_π^τ	(0.217, 0.807)	(0.217, 0.807)
$R_{D^*}^\tau(\times 10^3)$	(0.948, 1.352)	(0.948, 1.352)	R_π	(0.710, 1.212)	(0.710, 1.212)
$R_{D_s}^\tau(\times 10^3)$	(1.090, 1.682)	(1.090, 1.682)	R_{D_s}	(0.288, 0.378)	(0.288, 0.378)
$R_{D_s^*}^\tau(\times 10^3)$	(0.836, 1.191)	(0.836, 1.191)	$R_{D_s^*}$	(0.237, 0.250)	(0.237, 0.250)

TABLE VIII. Allowed ranges in $\mathcal{B}(B_c \to \tau\nu)$ with $V_{L,R}$, $S_{L,R}$, $\tilde{V}_{L,R}$, and $\tilde{S}_{L,R}$ NP couplings.

Observable	$V_{L,R}$ couplings	$S_{L,R}$ couplings	$\tilde{V}_{L,R}$ couplings	$\tilde{S}_{L,R}$ couplings
$\mathcal{B}(B_c \to \tau\nu)\times 10^2$	[1.97, 4.31]	[3.93, 15.88]	[1.83, 4.38]	[8.16, 13.77]

seem to affect any of the observables. The allowed ranges in each observable are given in Table V.

In the third scenario, we study the impact of new vector couplings $\tilde{V}_L$ and $\tilde{V}_R$, associated with right-handed neutrinos, on various observables. We first restrict the NP parameter space by imposing 2σ experimental constraints from the *BABAR* measured values of the ratio of branching ratios R_D, R_{D^*}, and $\mathcal{B}(B \to \tau\nu)$. We also impose 2σ constraints from the values of R_D^τ and $R_{D^*}^\tau$ that are estimated using the *BABAR* measured values of R_D and R_{D^*}, and $\mathcal{B}(B \to \tau\nu)$. The allowed ranges in $\tilde{V}_L$ and $\tilde{V}_R$ are shown in Fig. 5. The NP effects from $\tilde{V}_L$ and $\tilde{V}_R$ on various observables are shown in Fig. 6. We report the ranges in each observable in Table VI. We see significant deviation

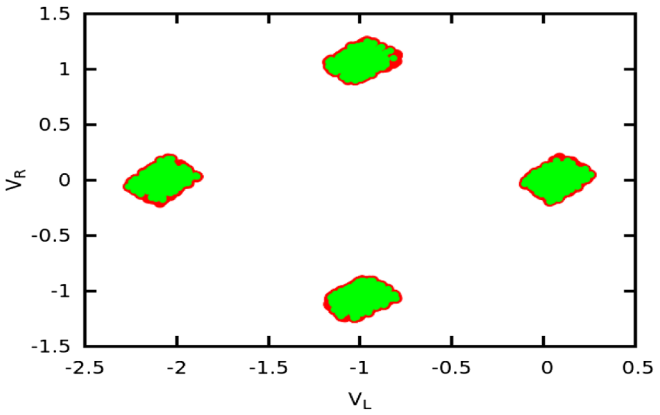

FIG. 8. Allowed ranges in (V_L, V_R) NP couplings after the Belle 2σ experimental constraint is imposed. The dark (red) region corresponds to the allowed ranges after R_D, R_{D^*}, and $\mathcal{B}(B \to \tau\nu)$ constraints are imposed, whereas the light (green) region corresponds to the allowed ranges of the NP couplings after an additional 2σ constraint from R_D^τ and $R_{D^*}^\tau$ is imposed.

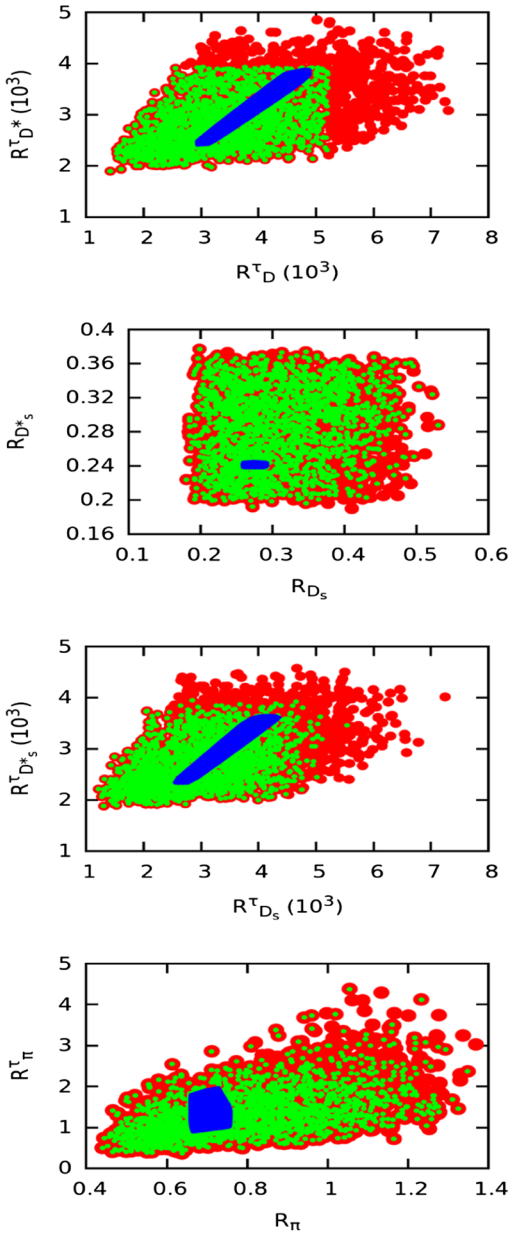

FIG. 9. Allowed ranges in various observables with V_L and V_R NP couplings of Fig. 8. Dark (red) regions represent the allowed range obtained by imposing 2σ constraints from Belle measured values of R_D, R_{D^*}, and $\mathcal{B}(B \to \tau\nu)$, whereas the light (green) regions represent the allowed range after 2σ additional constraints from R_D^τ and $R_{D^*}^\tau$ are imposed. The blue region corresponds to the 1σ allowed range within the SM.

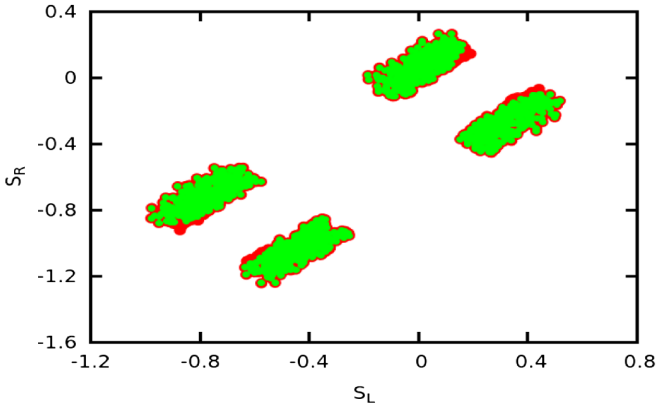

FIG. 10. Allowed ranges in (S_L, S_R) NP couplings after the Belle 2σ experimental constraint is imposed. The dark (red) region corresponds to the allowed ranges after R_D, R_{D^*}, and $\mathcal{B}(B \to \tau\nu)$ constraints are imposed, whereas the light (green) region corresponds to the allowed ranges of the NP couplings after an additional 2σ constraint from R^τ_D and $R^\tau_{D^*}$ is imposed.

of all the observables from the SM prediction, similar to the first scenario. Similar to scenario I, the deviation from the SM prediction is found to be more pronounced in the case of R_{D_s} and $R_{D_s^*}$. We observe that the ranges in $R^\tau_{D_s}$, $R^\tau_{D_s^*}$, and R^τ_π are reduced after the additional 2σ constraints from R^τ_D and $R^\tau_{D^*}$ are imposed. However, we see no or very little change in R_π, R_{D_s}, and $R_{D_s^*}$. Again, if only $\tilde{V}_L$-type NP couplings are present, then $\tilde{G}_V = \tilde{G}_A$ and the NP effect will cancel in $R^\tau_{D^{(*)}_{(s)}}$ and R^τ_π.

In the fourth scenario, we vary $\tilde{S}_L$ and $\tilde{S}_R$, new scalar couplings associated with right-handed neutrinos, while keeping others zero. The allowed ranges in $\tilde{S}_L$ and $\tilde{S}_R$ after imposing the 2σ constraints from the *BABAR* measured values are $\tilde{S}_L = [0.41, 0.50]$ and $\tilde{S}_R = [0.00, 0.01]$, respectively. We see that additional constraints from R^τ_D, $R^\tau_{D^*}$ do not have any effect on the allowed ranges of $\tilde{S}_L$ and $\tilde{S}_R$ obtained using the constraints from R_D, R_{D^*}, and $\mathcal{B}(B \to \tau\nu)$. The effect of these NP couplings on various observables are shown in Fig. 7. The allowed ranges in each observable are given in Table VII. Again, significant deviation from the SM expectation is seen for all the observables. Imposing the additional 2σ constraints from the new observables R^τ_D and $R^\tau_{D^*}$ does not seem to affect the observables in this scenario.

In Ref. [39], it was shown that the $B_c \to \tau\nu$ decay rate puts a severe constraint on NP scenarios involving scalar operators. In order to see the effect of $\mathcal{B}(B_c \to \tau\nu)$ on $V_{L,R}$, $S_{L,R}$, $\tilde{V}_{L,R}$, and $\tilde{S}_{L,R}$ NP couplings, we estimate the $B_c \to \tau\nu$ branching ratio using the NP couplings obtained by imposing 2σ constraints from *BABAR* measured values of R_D, R_{D^*}, and $\mathcal{B}(B \to \tau\nu)$. We show in Table VIII the range in $\mathcal{B}(B_c \to \tau\nu)$ for all four NP scenarios. Based on various

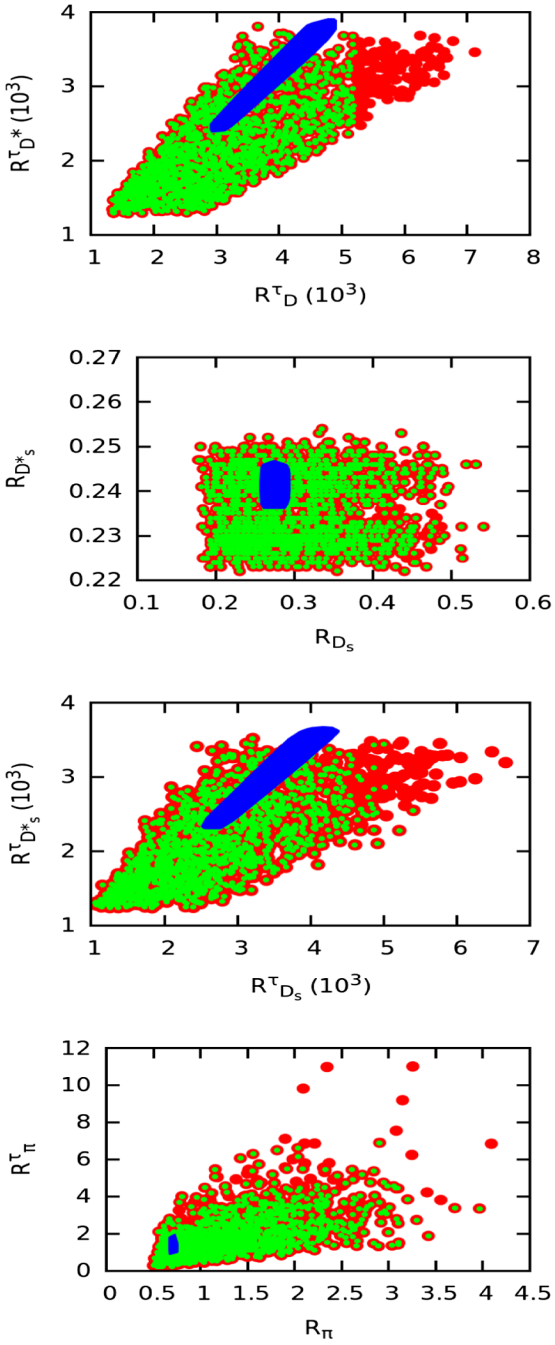

FIG. 11. Allowed ranges in various observables with the S_L and S_R NP couplings of Fig. 10. We show in dark (red) the allowed range in each observable after 2σ constraints from Belle measured values of R_D, R_{D^*}, and $\mathcal{B}(B \to \tau\nu)$ are imposed. Similarly, the allowed ranges in each observable are shown in light (green) after additional 2σ constraints from R^τ_D and $R^\tau_{D^*}$ are imposed. The blue region corresponds to the 1σ allowed range within the SM.

SM calculations [68–72], it can be inferred that no more than 5% of the total decay width of the B_c meson can be explained by the semi(taunic) decays of the B_c meson. The constraint, however, can be relaxed up to around 30% depending on the value of the total decay

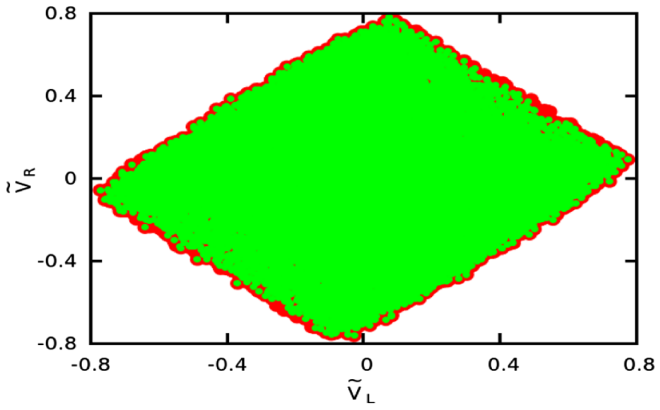

FIG. 12. Allowed ranges in $(\tilde{V}_L, \tilde{V}_R)$ NP couplings after the Belle 2σ experimental constraint is imposed. The dark (red) region corresponds to the allowed ranges after R_D, R_{D^*}, and $\mathcal{B}(B \to \tau\nu)$ constraints are imposed, whereas the light (green) region corresponds to the allowed ranges of the NP couplings after an additional 2σ constraint from R_D^τ and $R_{D^*}^\tau$ is imposed.

width of the B_c meson that is used as input for the SM calculation of various partonic transitions. If we assume that $\mathcal{B}(B_c \to \tau\nu)$ cannot be greater than 5%, then although $\tilde{S}_L$ and $\tilde{S}_R$ NP couplings can explain the anomalies in R_D, R_{D^*}, and $\mathcal{B}(B \to \tau\nu)$, it cannot simultaneously explain $\mathcal{B}(B_c \to \tau\nu)$. Even for the S_L and S_R NP couplings, a large part of the NP parameter space preferred by R_D, R_{D^*}, and $\mathcal{B}(B \to \tau\nu)$ can be excluded.

We observe that all the NP scenarios can accommodate the existing data on $b \to (u,c)\tau\nu$ decays. However, for $S_{L,R}$ and $\tilde{S}_{L,R}$ NP couplings, there are very few points that are compatible with the 2σ constraints from *BABAR* measurements. It is worth mentioning that precise measurements of R_{D_s}, $R_{D_s^*}$, R_π, and R_π^τ in the future will be crucial in distinguishing various NP structures.

B. Belle constraint

Now we wish to find the effect of (V_L, V_R)-, (S_L, S_R)-, $(\tilde{V}_L, \tilde{V}_R)$-, and $(\tilde{S}_L, \tilde{S}_R)$-type NP couplings on all the observables using experimental constraints from the Belle measurement. We consider four different NP scenarios similar to the *BABAR* analysis in Sec. III A. We first impose 2σ constraints from the Belle measured values of the ratio of branching ratios R_D, R_{D^*}, and $\mathcal{B}(B \to \tau\nu)$ to explore various NP scenarios. We again impose 2σ constraints from R_D^τ and $R_{D^*}^\tau$ that are estimated using the Belle measured values of R_D, R_{D^*}, and $\mathcal{B}(B \to \tau\nu)$ to see whether it is possible to constrain the NP parameter space even further. The allowed ranges of the NP couplings and their effects on various observables are shown in Figs. 8–15. In Figs. 8,10,12, and 14, we show the allowed ranges of (V_L, V_R), (S_L, S_R), $(\tilde{V}_L, \tilde{V}_R)$, and $(\tilde{S}_L, \tilde{S}_R)$ NP couplings after the 2σ constraint from Belle measured values is imposed. The dark (red) regions correspond to the allowed ranges of NP couplings that are obtained after the 2σ constraint from the measured values of R_D, R_{D^*}, and $\mathcal{B}(B \to \tau\nu)$ is imposed, whereas the light (green) region corresponds to the allowed ranges of NP couplings after additional 2σ constraints from the estimated values of R_D^τ

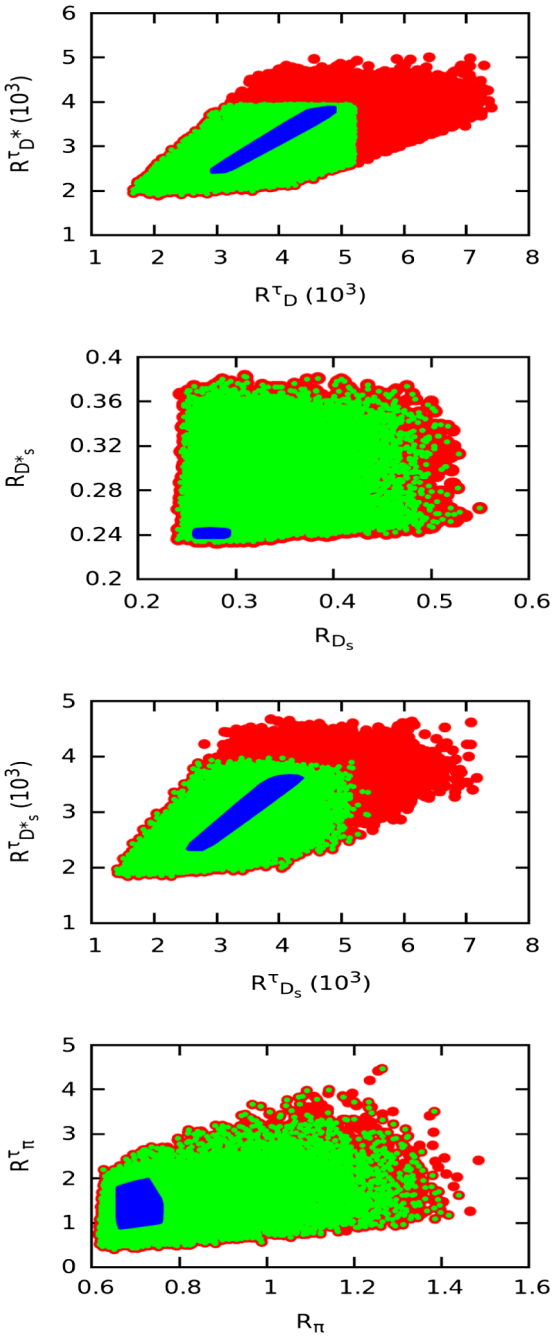

FIG. 13. Allowed ranges in various observables with the $\tilde{V}_L$ and $\tilde{V}_R$ NP couplings of Fig. 12. Dark (red) regions represent the allowed range obtained by imposing 2σ constraints from Belle measured values of R_D, R_{D^*}, and $\mathcal{B}(B \to \tau\nu)$, whereas the light (green) regions represent the allowed range after 2σ additional constraints from R_D^τ and $R_{D^*}^\tau$ are imposed. The blue region corresponds to the 1σ allowed range within the SM.

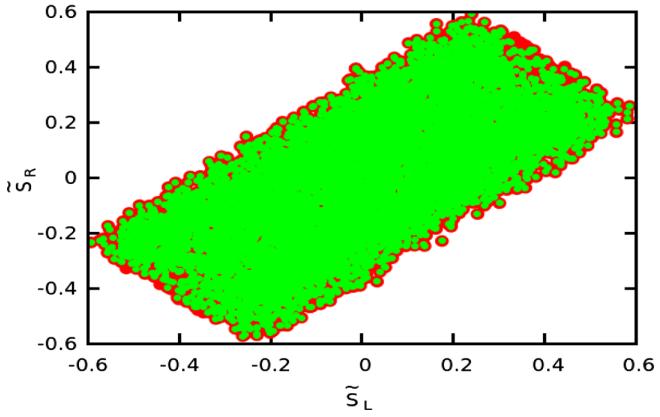

FIG. 14. Allowed ranges in $(\tilde{S}_L, \tilde{S}_R)$ NP couplings after the Belle 2σ experimental constraint is imposed. The dark (red) region corresponds to the allowed ranges after R_D, R_{D^*}, and $\mathcal{B}(B \to \tau\nu)$ constraints are imposed, whereas the light (green) region corresponds to the allowed ranges of the NP couplings after an additional 2σ constraint from R_D^τ and $R_{D^*}^\tau$ is imposed.

and $R_{D^*}^\tau$ are imposed. From Figs. 8,10,12, and 14, it is clear that the additional constraints from R_D^τ and $R_{D^*}^\tau$ reduce the NP parameter space to a very little extent. More precise data on V_{ub} will be crucial to constrain the NP parameter space even further.

The effects of NP on each observable under various scenarios are shown in Figs. 9,11,13, and 15. The deviation from the SM expectation is found to be significant in all four scenarios. For definiteness, we report the allowed ranges in each observable for each scenario in Tables IX–XII. We see that for (V_L, V_R) couplings, although the allowed ranges of $R_{D_s}^\tau$ and $R_{D_s^*}^\tau$ are reduced, there is no or very little change in the allowed ranges of R_π^τ, R_π, R_{D_s}, and $R_{D_s^*}$ after we impose 2σ constraints from R_D^τ and $R_{D^*}^\tau$. Similar results are observed for $(\tilde{V}_L, \tilde{V}_R)$ NP couplings as well. For (S_L, S_R)-type NP couplings, we find considerable reduction in the allowed range of R_π^τ, whereas there is no or very little change in the allowed ranges of $R_{D^*}^\tau$, $R_{D_s^*}^\tau$, R_{D_s}, $R_{D_s^*}$, and R_π after additional 2σ constraints from the estimated values of R_D^τ and $R_{D^*}^\tau$ are imposed. Similar results are obtained for $(\tilde{S}_L, \tilde{S}_R)$ NP couplings as well.

To see the effect of the $\mathcal{B}(B_c \to \tau\nu)$ constraint on various NP couplings, we estimate the range in $\mathcal{B}(B_c \to \tau\nu)$ using the $V_{L,R}$, $S_{L,R}$, $\tilde{V}_{L,R}$, and $\tilde{S}_{L,R}$ obtained by imposing the 2σ constraints from Belle measured values of R_D, R_{D^*}, and $\mathcal{B}(B \to \tau\nu)$. We report in Table XIII the range of $\mathcal{B}(B_c \to \tau\nu)$ obtained in all four scenarios. It is evident that a large part of $S_{L,R}$ and $\tilde{S}_{L,R}$ NP parameter space preferred by R_D, R_{D^*}, and $\mathcal{B}(B \to \tau\nu)$ can be excluded once the $\mathcal{B}(B_c \to \tau\nu) \leq 5\%$ constraint is imposed. Precise determination of the $B_c \to \tau\nu$ branching ratio in the future will be crucial to rule out various NP scenarios.

It is evident that all four NP scenarios not only accommodate the existing data on R_D, R_{D^*}, and $\mathcal{B}(B \to \tau\nu)$, but also accommodate the newly estimated data on R_D^τ and $R_{D^*}^\tau$. It is worth mentioning that the range of R_π^τ obtained in each scenario exceeds the upper limit on $R_\pi^\tau < 2.62$ [55] estimated using the combined Belle result for $\mathcal{B}(B \to \tau\nu)$ and the upper limit for $\mathcal{B}(B \to \pi\tau\nu) < 2.5 \times 10^{-4}$ [73].

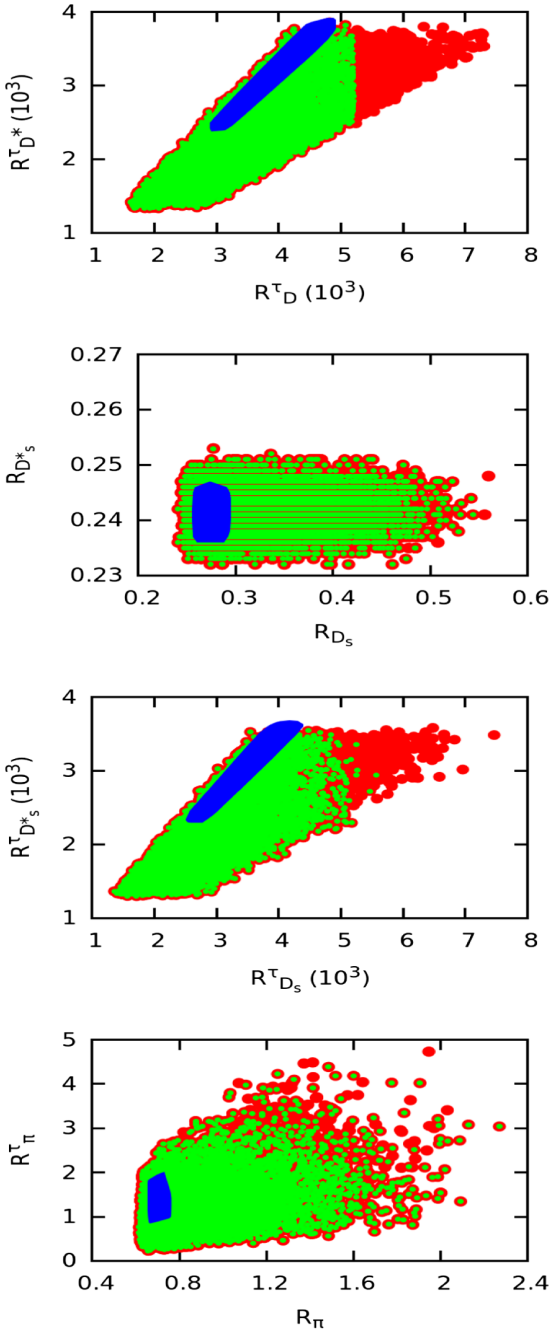

FIG. 15. Allowed ranges in various observables with the $\tilde{S}_L$ and $\tilde{S}_R$ NP couplings of Fig. 14. We show in dark (red) the allowed range in each observable after 2σ constraints from Belle measured values of R_D, R_{D^*}, and $\mathcal{B}(B \to \tau\nu)$ are imposed. Again, we show in light (green) the allowed range after additional 2σ constraints from R_D^τ and $R_{D^*}^\tau$ are imposed. The blue region corresponds to the 1σ allowed range within the SM.

TABLE IX. Allowed ranges in various observables with the (V_L, V_R) NP couplings of Fig. 8. The ranges reported in Column I represent the allowed values of each observable after constraints from Belle measured values of R_D, R_{D^*}, and $\mathcal{B}(B \to \tau\nu)$ are imposed, whereas the ranges in Column II represent the allowed values after additional 2σ constraints from R^τ_D and $R^\tau_{D^*}$ are imposed.

Observable	Column I	Column II	Observable	Column I	Column II
$R^\tau_D(\times 10^3)$	(1.417, 7.304)	(1.417, 5.198)	R^τ_π	(0.359, 4.382)	(0.359, 4.382)
$R^\tau_{D^*}(\times 10^3)$	(1.897, 4.856)	(1.897, 3.932)	R_π	(0.440, 1.369)	(0.440, 1.349)
$R^\tau_{D_s}(\times 10^3)$	(1.212, 7.247)	(1.212, 5.534)	R_{D_s}	(0.180, 0.530)	(0.180, 0.530)
$R^\tau_{D_s^*}(\times 10^3)$	(1.880, 4.576)	(1.880, 3.949)	$R_{D_s^*}$	(0.190, 0.377)	(0.192, 0.377)

TABLE X. Allowed ranges in various observables with (S_L, S_R) NP couplings from Fig. 10. The ranges reported in Column I represent the allowed values of each observable after constraints from Belle measured values of R_D, R_{D^*}, and $\mathcal{B}(B \to \tau\nu)$ are imposed, whereas the ranges in Column II represent the allowed values after additional 2σ constraints from R^τ_D and $R^\tau_{D^*}$ are imposed.

Observable	Column I	Column II	Observable	Column I	Column II
$R^\tau_D(\times 10^3)$	(1.336, 7.122)	(1.336, 5.199)	R^τ_π	(0.207, 11.012)	(0.207, 6.901)
$R^\tau_{D^*}(\times 10^3)$	(1.287, 3.804)	(1.287, 3.804)	R_π	(0.496, 4.091)	(0.496, 3.964)
$R^\tau_{D_s}(\times 10^3)$	(1.060, 6.669)	(1.060, 5.406)	R_{D_s}	(0.177, 0.541)	(0.177, 0.541)
$R^\tau_{D_s^*}(\times 10^3)$	(1.238, 3.532)	(1.238, 3.532)	$R_{D_s^*}$	(0.222, 0.254)	(0.222, 0.254)

TABLE XI. Allowed ranges in various observables with the $(\tilde{V}_L, \tilde{V}_R)$ NP couplings of Fig. 12. The ranges reported in Column I represent the allowed values of each observable after constraints from Belle measured values of R_D, R_{D^*}, and $\mathcal{B}(B \to \tau\nu)$ are imposed, whereas the ranges in Column II represent the allowed values after additional 2σ constraints from R^τ_D and $R^\tau_{D^*}$ are imposed.

Observable	Column I	Column II	Observable	Column I	Column II
$R^\tau_D(\times 10^3)$	(1.665, 7.402)	(1.665, 5.200)	R^τ_π	(0.398, 4.471)	(0.398, 4.471)
$R^\tau_{D^*}(\times 10^3)$	(1.889, 5.008)	(1.889, 3.942)	R_π	(0.616, 1.485)	(0.616, 1.440)
$R^\tau_{D_s}(\times 10^3)$	(1.406, 7.168)	(1.406, 5.429)	R_{D_s}	(0.241, 0.550)	(0.241, 0.550)
$R^\tau_{D_s^*}(\times 10^3)$	(1.846, 4.675)	(1.846, 3.974)	$R_{D_s^*}$	(0.233, 0.383)	(0.233, 0.383)

TABLE XII. Allowed ranges in various observables with $(\tilde{S}_L, \tilde{S}_R)$ NP couplings from Fig. 14. The ranges reported in Column I represent the allowed values of each observable after constraints from Belle measured values of R_D, R_{D^*}, and $\mathcal{B}(B \to \tau\nu)$ are imposed, whereas the ranges in Column II represent the allowed values after additional 2σ constraints from R^τ_D and $R^\tau_{D^*}$ are imposed.

Observable	Column I	Column II	Observable	Column I	Column II
$R^\tau_D(\times 10^3)$	(1.622, 7.301)	(1.622, 5.200)	R^τ_π	(0.229, 4.732)	(0.229, 4.387)
$R^\tau_{D^*}(\times 10^3)$	(1.333, 3.857)	(1.333, 3.857)	R_π	(0.616, 2.271)	(0.616, 2.271)
$R^\tau_{D_s}(\times 10^3)$	(1.352, 7.465)	(1.352, 5.564)	R_{D_s}	(0.241, 0.560)	(0.241, 0.544)
$R^\tau_{D_s^*}(\times 10^3)$	(1.297, 3.583)	(1.297, 3.563)	$R_{D_s^*}$	(0.232, 0.253)	(0.232, 0.253)

TABLE XIII. Allowed ranges in $\mathcal{B}(B_c \to \tau\nu)$ with $V_{L,R}$, $S_{L,R}$, $\tilde{V}_{L,R}$, and $\tilde{S}_{L,R}$ NP couplings.

Observable	$V_{L,R}$ couplings	$S_{L,R}$ couplings	$\tilde{V}_{L,R}$ couplings	$\tilde{S}_{L,R}$ couplings
$\mathcal{B}(B_c \to \tau\nu) \times 10^2$	[1.42, 4.29]	[1.00, 11.47]	[1.73, 4.22]	[1.73, 10.49]

More precise data on $\mathcal{B}(B \to \tau\nu)$ and $\mathcal{B}(B \to \pi\tau\nu)$ in the future will definitely help constrain the NP parameter space even further. Here, too, more precise measurements are required to distinguish various NP structures.

IV. CONCLUSION

Lepton flavor universality violation has been observed in various semileptonic B meson decays. The measured values of R_D and R_{D^*} exceed the SM expectation by

1.9σ and 3.3σ, respectively. The HFAG Collaboration reported the combined deviation from the SM prediction to be at the level of 4σ. Similar tensions have been observed in $B \to (K, K^*)ll$ and $B_s \to \phi ll$ decays mediated via the $b \to sll$ transition process as well. Many phenomenological studies have been performed in order to explain these discrepancies. Measurements of $B \to \tau\nu$ and $B \to (D, D^*)\tau\nu$ decays suffer τ detection and identification systematics. To examine this possibility, very recently, in Ref. [55], the authors introduced two new observables, namely, R_D^τ and $R_{D^*}^\tau$, where the τ detection and identification systematics will largely cancel. The estimated values of R_D^τ and $R_{D^*}^\tau$ are consistent with the SM prediction, although there is discrepancy between the measured R_D and R_{D^*} with the SM prediction. This may occur for a class of NP which affect R_D, R_{D^*} and $B \to \tau\nu$ decays. In Ref. [55], the authors consider the type II 2HDM model to illustrate these points.

In this paper, we use an effective field theory in the presence of NP to explore various NP couplings. First, we consider the constraints from the measured values of R_D, R_{D^*}, and $\mathcal{B}(B \to \tau\nu)$ to see various NP effects on these new observables. Second, we see whether it is possible to constrain the NP parameter space even further by using additional constraints from the estimated values of R_D^τ and $R_{D^*}^\tau$ since these ratios are consistent with the SM values. We study the effect of new physics couplings on various observables related to $B_s \to (D_s, D_s^*)\tau\nu$ and $B \to \pi\tau\nu$ decays as well. We analyze *BABAR* and Belle data separately so as to make a comparison between the two. The main results of our analysis are summarized below.

We first study the impact of NP couplings on various observables using 2σ constraints from *BABAR* measured values of R_D, R_{D^*}, and $\mathcal{B}(B \to \tau\nu)$. We consider four different NP scenarios. We find significant deviation from the SM prediction in each observable for each scenario. We find that, although each of the four NP scenarios can simultaneously explain all the existing data on $b \to u$ and $b \to c$ leptonic and semileptonic B meson decays, there are very few points that are compatible within the 2σ constraints from *BABAR* measurements for (S_L, S_R) and $(\tilde{S}_L, \tilde{S}_R)$ NP couplings. Our second point was to see whether it is possible to constrain the NP parameter space even further by imposing constraints from the newly constructed observables R_D^τ and $R_{D^*}^\tau$. We see that the additional constraint from the new observables R_D^τ and $R_{D^*}^\tau$ does not constrain (S_L, S_R) and $(\tilde{S}_L, \tilde{S}_R)$ NP parameter space. However, for (V_L, V_R) and $(\tilde{V}_L, \tilde{V}_R)$ NP couplings, the allowed ranges in $R_{D_s}^\tau$, $R_{D_s^*}^\tau$, and R_π^τ are considerably reduced after the additional 2σ constraint from R_D^τ and $R_{D^*}^\tau$ is imposed.

We do the same analysis using the Belle measured values. We first constrain the NP parameter space using 2σ constraints from Belle measured values of R_D, R_{D^*}, and $\mathcal{B}(B \to \tau\nu)$. The deviation from the SM expectation is found to be significant in all four scenarios. We find that for (V_L, V_R) couplings, although the allowed ranges in $R_{D_s}^\tau$ and $R_{D_s^*}^\tau$ are reduced, there is no or very little change in R_π^τ, R_π, R_{D_s}, and $R_{D_s^*}$ allowed ranges after we impose 2σ constraints from R_D^τ and $R_{D^*}^\tau$. Similar results are obtained for $(\tilde{V}_L, \tilde{V}_R)$ NP couplings as well. For (S_L, S_R)-type NP couplings, the allowed range in R_π^τ reduces considerably, whereas there is no or very little change in $R_{D^*}^\tau$, $R_{D_s^*}^\tau$, R_{D_s}, $R_{D_s^*}$, and R_π allowed ranges after additional 2σ constraints from the estimated values of R_D^τ and $R_{D^*}^\tau$ are imposed. Similar results are obtained for $(\tilde{S}_L, \tilde{S}_R)$ NP couplings as well. It should be mentioned that new physics couplings $S_{L,R}$ and $\tilde{S}_{L,R}$ are much more compatible with Belle data than with the *BABAR* data.

Although current measurements from *BABAR* and Belle suggest the presence of NP, NP is yet to be confirmed. Both experimental and theoretical precision in these B decay modes are necessary for a reliable interpretation of NP signals if NP is indeed present. Retaining our current approach, we could sharpen our estimates after improved measurement of V_{ub} is available. These newly defined observables may, in the future, play a crucial role in identifying the nature of NP couplings in $b \to (u, c)\tau\nu$ decays. Again, precise data on $\mathcal{B}(B \to \pi\tau\nu)$ will put additional constraints on the NP parameter space. Similarly, measurements of R_{D_s} and $R_{D_s^*}$ will also help in identifying the nature of NP couplings in $b \to c\tau\nu$ decays. Moreover, precise calculations of the B_c lifetime and measurements of the branching fractions of its various decay channels in the future should help constrain the NP parameter space even further.

[1] S. Fajfer, J. F. Kamenik, I. Nisandzic, and J. Zupan, Phys. Rev. Lett. **109**, 161801 (2012).
[2] S. Fajfer, J. F. Kamenik, and I. Nisandzic, Phys. Rev. D **85**, 094025 (2012).
[3] W. S. Hou, Phys. Rev. D **48**, 2342 (1993).
[4] A. G. Akeroyd and S. Recksiegel, J. Phys. G **29**, 2311 (2003).
[5] M. Tanaka, Z. Phys. C **67**, 321 (1995).
[6] U. Nierste, S. Trine, and S. Westhoff, Phys. Rev. D **78**, 015006 (2008).

[7] T. Miki, T. Miura, and M. Tanaka, arXiv:hep-ph/0210051.
[8] A. W. E. Kaffas, P. Osland, and O. M. Ogreid, Phys. Rev. D **76**, 095001 (2007).
[9] O. Deschamps, S. Descotes-Genon, S. Monteil, V. Niess, S. T'Jampens, and V. Tisserand, Phys. Rev. D **82**, 073012 (2010).
[10] G. Blankenburg and G. Isidori, Eur. Phys. J. Plus **127**, 85 (2012).
[11] G. D'Ambrosio, G. F. Giudice, G. Isidori, and A. Strumia, Nucl. Phys. **B645**, 155 (2002).
[12] A. J. Buras, M. V. Carlucci, S. Gori, and G. Isidori, J. High Energy Phys. 10 (2010) 009.
[13] A. Pich and P. Tuzon, Phys. Rev. D **80**, 091702 (2009).
[14] M. Jung, A. Pich, and P. Tuzon, J. High Energy Phys. 11 (2010) 003.
[15] A. Crivellin, C. Greub, and A. Kokulu, Phys. Rev. D **86**, 054014 (2012).
[16] A. Datta, M. Duraisamy, and D. Ghosh, Phys. Rev. D **86**, 034027 (2012).
[17] M. Duraisamy and A. Datta, J. High Energy Phys. 09 (2013) 059.
[18] M. Duraisamy, P. Sharma, and A. Datta, Phys. Rev. D **90**, 074013 (2014).
[19] B. Bhattacharya, A. Datta, D. London, and S. Shivashankara, Phys. Lett. B **742**, 370 (2015).
[20] B. Bhattacharya, A. Datta, J. P. Guvin, D. London, and R. Watanabe, J. High Energy Phys. 01 (2017) 015.
[21] P. Biancofiore, P. Colangelo, and F. De Fazio, Phys. Rev. D **87**, 074010 (2013).
[22] A. Crivellin, Phys. Rev. D **81**, 031301 (2010).
[23] A. Celis, M. Jung, X.-Q. Li, and A. Pich, J. High Energy Phys. 01 (2013) 054.
[24] X.-G. He and G. Valencia, Phys. Rev. D **87**, 014014 (2013).
[25] R. Dutta, A. Bhol, and A. K. Giri, Phys. Rev. D **88**, 114023 (2013).
[26] M. Tanaka and R. Watanabe, Prog. Theor. Exp. Phys. **2017**, 013B05 (2017).
[27] N. G. Deshpande and X. G. He, Eur. Phys. J. C **77**, 134 (2017).
[28] X. Q. Li, Y. D. Yang, and X. Zhang, J. High Energy Phys. 08 (2016) 054.
[29] D. Du, A. X. El-Khadra, S. Gottlieb, A. S. Kronfeld, J. Laiho, E. Lunghi, R. S. Van de Water, and R. Zhou, Phys. Rev. D **93**, 034005 (2016).
[30] F. U. Bernlochner, Phys. Rev. D **92**, 115019 (2015).
[31] A. Soffer, Mod. Phys. Lett. A **29**, 1430007 (2014).
[32] M. Bordone, G. Isidori, and D. van Dyk, Eur. Phys. J. C **76**, 360 (2016).
[33] D. Bardhan, P. Byakti, and D. Ghosh, J. High Energy Phys. 01 (2017) 125.
[34] A. K. Alok, D. Kumar, S. Kumbhakar, and S. U. Sankar, Phys. Rev. D **95**, 115038 (2017).
[35] M. A. Ivanov, J. G. Körner, and C. T. Tran, Phys. Rev. D **92**, 114022 (2015).
[36] M. A. Ivanov, J. G. Körner, and C. T. Tran, Phys. Rev. D **94**, 094028 (2016).
[37] S. M. Boucenna, A. Celis, J. Fuentes-Martin, A. Vicente, and J. Virto, Phys. Lett. B **760**, 214 (2016).
[38] S. M. Boucenna, A. Celis, J. Fuentes-Martin, A. Vicente, and J. Virto, J. High Energy Phys. 12 (2016) 059.
[39] R. Alonso, B. Grinstein, and J. M. Camalich, Phys. Rev. Lett. **118**, 081802 (2017).
[40] R. M. Woloshyn, Proc. Sci., Hadron 2013 (**2013**) 203.
[41] S. Shivashankara, W. Wu, and A. Datta, Phys. Rev. D **91**, 115003 (2015).
[42] T. Gutsche, M. A. Ivanov, J. G. Körner, V. E. Lyubovitskij, P. Santorelli, and N. Habyl, Phys. Rev. D **91**, 074001 (2015); **91**, 119907 (2015).
[43] W. Detmold, C. Lehner, and S. Meinel, Phys. Rev. D **92**, 034503 (2015).
[44] R. Dutta, Phys. Rev. D **93**, 054003 (2016).
[45] A. Matyja *et al.* (Belle Collaboration), Phys. Rev. Lett. **99**, 191807 (2007).
[46] A. Bozek *et al.* (Belle Collaboration), Phys. Rev. D **82**, 072005 (2010).
[47] M. Huschle *et al.* (Belle Collaboration), Phys. Rev. D **92**, 072014 (2015).
[48] J. P. Lees *et al.* (*BABAR* Collaboration), Phys. Rev. Lett. **109**, 101802 (2012).
[49] J. P. Lees *et al.* (*BABAR* Collaboration), Phys. Rev. D **88**, 072012 (2013).
[50] R. Aaij *et al.* (LHCb Collaboration), Phys. Rev. Lett. **115**, 111803 (2015); **115**, 159901(A) (2015).
[51] Y. Sato *et al.* (Belle Collaboration), Phys. Rev. D **94**, 072007 (2016).
[52] Y. Amhis *et al.* (Heavy Flavor Averaging Group (HFAG) Collaboration), arXiv:1412.7515 and online update at http://www.slac.stanford.edu/xorg/hfag/.
[53] J. P. Lees *et al.* (*BABAR* Collaboration), Phys. Rev. D **88**, 031102 (2013).
[54] B. Kronenbitter *et al.* (Belle Collaboration), Phys. Rev. D **92**, 051102 (2015).
[55] S. Nandi, S. K. Patra, and A. Soni, arXiv:1605.07191.
[56] T. Bhattacharya, V. Cirigliano, S. D. Cohen, A. Filipuzzi, M. Gonzalez-Alonso, M. L. Graesser, R. Gupta, and H.-W. Lin, Phys. Rev. D **85**, 054512 (2012).
[57] V. Cirigliano, J. Jenkins, and M. Gonzalez-Alonso, Nucl. Phys. **B830**, 95 (2010).
[58] A. Bhol, Europhys. Lett. **106**, 31001 (2014).
[59] C. Patrignani *et al.* (Particle Data Group Collaboration), Chin. Phys. C **40**, 100001 (2016).
[60] J. Beringer *et al.* (Particle Data Group Collaboration), Phys. Rev. D **86**, 010001 (2012).
[61] A. Bazavov *et al.* (Fermilab Lattice and MILC Collaborations), Phys. Rev. D **85**, 114506 (2012).
[62] H. Na, C. J. Monahan, C. T. H. Davies, R. Horgan, G. P. Lepage, and J. Shigemitsu, Phys. Rev. D **86**, 034506 (2012).
[63] See http://www.latticeaverages.org.
[64] A. Khodjamirian, T. Mannel, N. Offen, and Y.-M. Wang, Phys. Rev. D **83**, 094031 (2011).
[65] W. Dungel *et al.* (Belle Collaboration), Phys. Rev. D **82**, 112007 (2010).
[66] B. Aubert *et al.* (*BABAR* Collaboration), Phys. Rev. Lett. **104**, 011802 (2010).

[67] R. N. Faustov and V. O. Galkin, Phys. Rev. D **87**, 034033 (2013).
[68] I. I. Y. Bigi, Phys. Lett. B **371**, 105 (1996).
[69] M. Beneke and G. Buchalla, Phys. Rev. D **53**, 4991 (1996).
[70] C. H. Chang, S. L. Chen, T. F. Feng, and X. Q. Li, Phys. Rev. D **64**, 014003 (2001).
[71] S. S. Gershtein, V. V. Kiselev, A. K. Likhoded, and A. V. Tkabladze, Usp. Fiz. Nauk **165**, 3 (1995) [Phys. Usp. **38**, 1 (1995)].
[72] V. V. Kiselev, A. E. Kovalsky, and A. K. Likhoded, Nucl. Phys. **B585**, 353 (2000).
[73] P. Hamer *et al.* (Belle Collaboration), Phys. Rev. D **93**, 032007 (2016).